High-Resolution DWI in Brain and Spinal Cord with *syngo* RESOLVE[1]

Julien Cohen-Adad

Department of Electrical Engineering, Ecole Polytechnique de Montreal, QC, Canada
A. A. Martinos Center for Biomedical Imaging, Massachusetts General Hospital, Harvard Medical School, Charlestown, MA, USA

Abstract

In this paper we present some applications of the *syngo* RESOLVE[1] sequence that enable high-resolution diffusion-weighted imaging. The sequence is based on a readout-segmented EPI strategy, allowing susceptibility distortions and T2* blurring to be minimized. The RESOLVE[1] sequence can be combined with other acquisition strategies such as reduced field-of-view (FOV) and parallel imaging, to provide state-of-the-art tractography of the full brain and cervical spinal cord. The RESOLVE[1] sequence could be of particular interest for ultra high field systems where artifacts due to susceptibility and reduced T2 values are more severe. At all field strengths, the sequence promises to be useful in a number of clinical applications to characterize the diffusion properties of pathology with high resolution and a low level of image artifact.

1. Introduction

1.1. Diffusion-weighted imaging

Diffusion-weighted MRI makes it possible to map white matter architecture in the central nervous system based on the measurement of water diffusion [11]. The technique works by using MRI sequences that are sensitized to the microscopic motion of water molecules, which are in constant motion in biological tissues (Brownian motion). Using the well-known pulse sequence introduced by Stejskal and Tanner in 1965 [29], it is possible to quantify the extent of water displacement in a given direction. This sequence consists of magnetic field gradient pulses (diffusion-encoding gradients) that are applied before and after a 180° radiofrequency (RF) refocusing pulse. The first gradient pulse dephases the precessing nuclear spins that generate the signal in MRI. In the theoretical case of static molecules, the second gradient pulse completely rephases the spins and there is no attenuation due to the application of the gradients. However, if water molecules move during the application of this pair of gradients, spins are dephased and signal decreases as a function of the magnitude of the displacement, leading to a so-called diffusion-weighted signal. The magnitude by which the signal is weighted by diffusion is dictated by the so-called *b-value*, which depends on the length and amplitude of the applied diffusion-encoding gradients, as well as the duration between the first and the second gradient pulse (also called diffusion time). By applying diffusion gradients in various directions (e.g., 20 directions equally sampled on a sphere), it is possible to estimate the rate and direction of water diffusion. For example in pure water, molecules diffuse equally in all directions, hence the diffusion is described as *isotropic*. Conversely, in mesenchymal structures such as the white matter or muscles, water diffuses preferentially along the direction of the fiber. In such a case, the diffusion is *anisotropic* [3].

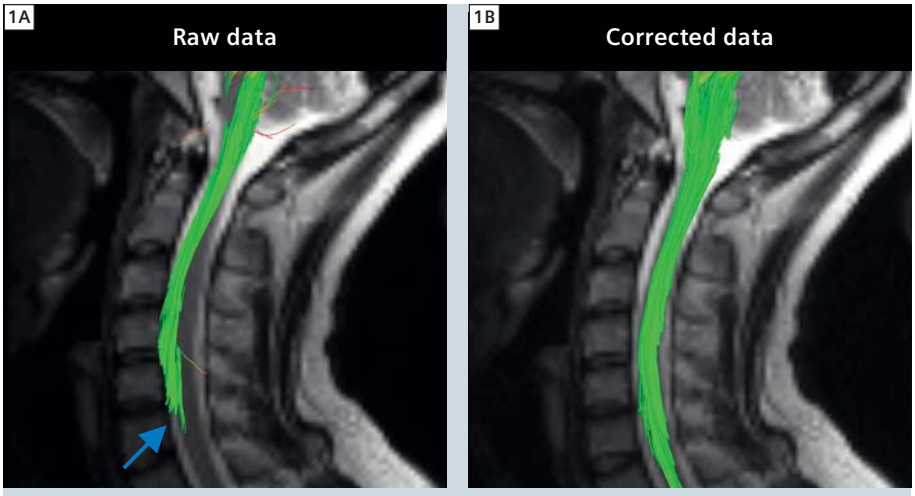

1 Tractography in a healthy subject, overlaid on a distortion-free anatomical image (fast spin echo). **(1A)** shows tractography performed on the raw data (i.e., without correction). **(1B)** shows tractography performed on the same dataset, after distortion correction using the reversed-gradient technique [13]. A false apparent interruption of the tracts is observed on the data hampered by susceptibility distortions. Acquisition was performed using the standard EPI sequence with the following parameters: sagittal orientation, TR/TE = 4000/86 ms, 1.8 mm isotropic, R = 2 acceleration. Tractography was seeded from a slice located at C1 vertebral level.

[1]The software is pending 510(k) clearance, and is not yet commercially available in the United States and in other countries.

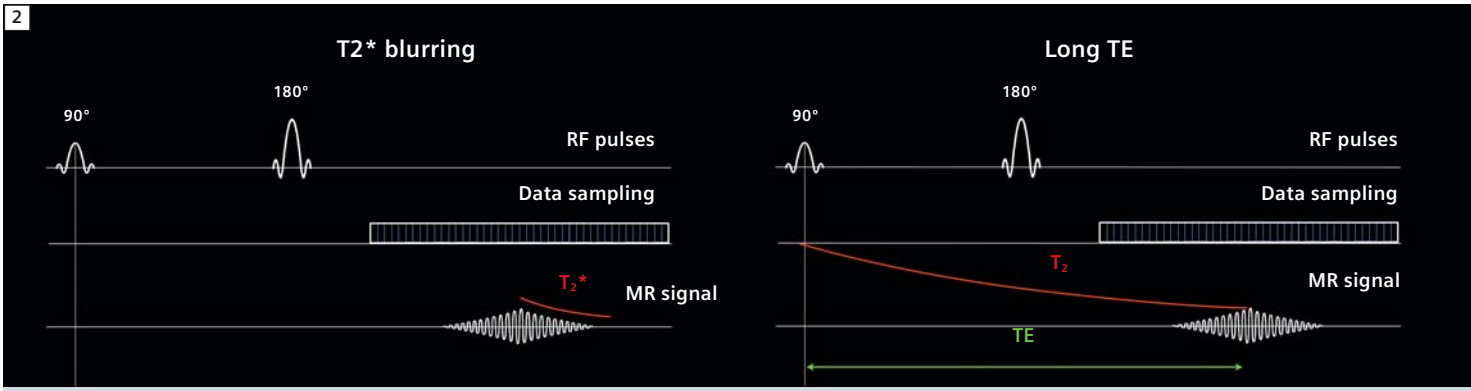

2 The left panel illustrates the origin of the T2* blurring effect, which is caused by T2* dephasing during *k*-space (raw data) sampling. The right panel illustrates the consequence of a long TE due to the combination of the diffusion-encoding gradients and the extended data sampling interval, resulting in low SNR data.

1.2. DTI and tractography

After acquiring a set of diffusion-weighted data, it is possible to compute a parametric model representing the main diffusion direction at each voxel [2]. This type of model is described by a tensor and is usually represented graphically as a 3D ellipsoid. This technique is known as Diffusion Tensor Imaging (DTI) and makes it possible to derive metrics such as fractional anisotropy (FA), mean diffusivity and axial and radial diffusivities. These metrics are relevant as they have been shown to correlate with demyelination and axonal degeneration [28] and can therefore be used to obtain markers of demyelination in multiple sclerosis [26], spinal cord injury [7] or amyotrophic lateral sclerosis [8].

Having modeled the diffusion tensor, it is possible to reconstruct global axonal pathways by linking every voxel with a similar eigenvector (principal axis of the diffusion tensor) to its neighbors. This procedure is called fiber tracking or tractography [18]. It should be mentioned however that the reconstructed fiber bundles do not represent *real* axonal tracts but rather represent the path where water diffuses preferentially. It is therefore an indirect measure of axon orientation. Hence, tractography results should be handled with care since they may not represent the real pathway of axons [14]. For instance, false negatives could be induced by the presence of crossing fibers, which would artificially decrease the FA and stop the tracking procedure. Inversely, false positives could be induced by fibrous structures such as scar tissue, in which water diffusion also has anisotropic properties [27]. In such cases, fiber tracking can become fiber *tricking*.

To illustrate the need for caution, Figure 1 shows an example of tractography performed in a healthy subject, before and after correction for susceptibility artifacts, which can induce strong image distortions in the phase-encoding direction (antero-posterior in this example). On the 'raw data' (1A), a false apparent interruption of the tracts is clearly observed, and can be misinterpreted as an interruption of the white matter tracts. However, this apparent interruption is simply due to susceptibility distortions, as can be seen on the 'corrected data' (1B). This result suggests two things: *(I)* a careful assessment of the image data is essential before further processing is applied and *(II)* susceptibility-induced distortions should be minimized by an appropriate choice of data acquisition technique. This might ultimately reduce the need for quality assessment, which is not often possible in clinical routine. This brings us to the next section on how to reduce susceptibility artifact during the acquisition.

1.3. Artifacts in diffusion-weighted imaging

In this section we will mostly focus on susceptibility artifacts and T2* blurring. Other artifacts exist in diffusion-weighted imaging [15], but are not in the scope of the presence article.

Single-shot echo planar imaging (ss-EPI) is an ultra-fast imaging sequence that makes it possible to acquire a full slice within a single repetition time (TR) [16]. To achieve this, spatial encoding gradients are played out rapidly along two gradient axes (e.g. X and Y) in order to sample all raw data (or *k*-space) points in a 'single shot' after an RF excitation pulse. By applying the EPI readout directly after the excitation pulse, a gradient echo image can be generated. Alternatively, an RF refocusing pulse can be inserted between the excitation and EPI readout to produce a spin echo image, which has reduced susceptibility-induced signal loss, but has the same sensitivity to susceptibility-based distortions. An oscillating readout gradient is applied along one axis (e.g. X), consisting of a series of gradient pulses with alternating polarity and each of these readout gradient pulses is used to sample a single line of *k*-space. A short phase-encoding gradient or 'blip' is applied along an orthogonal gradient axis (e.g. Y), so that each readout gradient corresponds to a different line of *k*-space in the Y direction. While acquisition of a full line a *k*-space in the read-

out direction is obtained rapidly (in about 1 ms), the acquisition of *k*-space data along the phase-encoding direction takes much more time. For example, for a 128×128 matrix, acquisition of the full *k*-space can take more than 100 ms. During that time, spins experience dephasing due to local B_0-inhomogeneities. These undesirable inhomogeneities are typically induced at interfaces between structures with different susceptibility properties, such as air/tissue or bone/muscle. As a result, phase errors accumulate in the phase-encoding direction, causing geometric distortions in the reconstructed image in that direction. EPI sequences are fast and particularly appropriate for diffusion-weighted experiments [31] where multiple datasets need to be acquired in a clinically acceptable time with low sensitivity to motion-induced phase error [17]. However single-shot EPI also has the disadvantage that it is particularly sensitive to susceptibility-related geometric distortions. Reduction of susceptibility artifacts can be achieved by sampling the *k*-space faster, which decreases the accumulation of the phase errors. Faster acquisition can be achieved by reducing the echo spacing, which is defined as the total time between the application of two phase-encode blips. Echo spacing can be reduced by *(I)* increasing the readout bandwidth, *(II)* reducing the number of phase lines by reducing the FOV (because the sampling density in *k*-space defines the FOV in the image domain) and *(III)* combining several subsampled *k*-space acquisitions (multi-shot). In addition to susceptibility artifacts, T2* blurring can be induced due to the relatively long sampling of *k*-space, during which T2* relaxation occur (Figure 2, left). This effect is more pronounced in regions with large B_0 inhomogeneities. Another undesirable effect of the long sampling is that it will impose a relatively long echo time (TE) (Figure 2, right). As a result, the recorded signal amplitude will be small due to the relatively short transverse relaxation (T2) in white matter (about 70 ms at 3T). This effect is critical since SNR is proportional to exp(-TE/T2), therefore even a small increase of TE (several ms) can substantially reduce the signal-to-noise ratio (SNR).

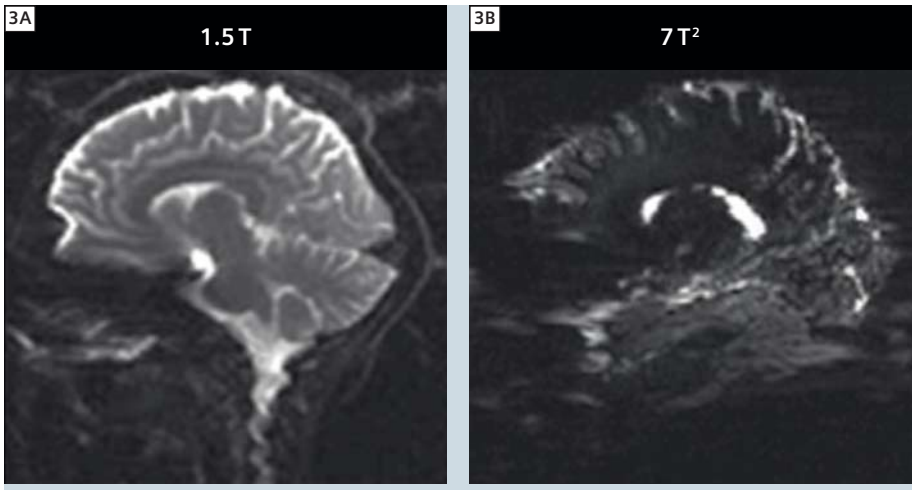

3 Comparison of single-shot EPI at 1.5T **(3A)** and 7T[2] **(3B)**.

4 Benefits of faster sampling for: *(I)* reducing susceptibility distortions (less accumulation of phase errors), *(II)* reducing T2* blurring (faster sampling) and *(III)* enabling shorter TE (due to the faster sampling of *k*-space, which in turn brings the center of the readout window closer to the 180° pulse).

All these limitations become even more problematic at higher field, where T2 is reduced (about 50 ms at 7T) and B_0 homogeneity is more difficult to achieve, resulting in a greater level of susceptibility artifact. Figure 3 shows an example of the high-field degradation in image quality when using the standard single-shot EPI technique at 1.5T and 7T[2].

To summarize, the main issues encountered with diffusion-weighting EPI are:

- **Susceptibility artifacts**, which are caused by an accumulation of phase error during the readout, leading to image distortions.
- **T2* blurring**, which is caused by the long data sampling interval during the readout, leading to a broadening of the point spread function and a blurring of the reconstructed image.
- **Long TE**, which is imposed by a combination of the diffusion-encoding gradients and the long data sampling interval and results in low SNR.

These three arguments provide motivation for a reduction in the sampling time, which will address all these issues, as illustrated in Figure 4.

[2]The 7T system is a research system only. It cannot be used outside of a research study.

2. Multi-shot techniques and *syngo* RESOLVE[1]

As described in the previous section, susceptibility artifacts and T2* blurring can be reduced by decreasing the sampling time (or the effective echo spacing). In EPI, this can be done by skipping lines of *k*-space in the phase-encoding direction (also called interleaved EPI). Multi-shot techniques consist of acquiring several sub-sampled images and combining them to reconstruct a full *k*-space data set. An example of a 2-shot interleaved EPI acquisition is illustrated in Figure 5. In this approach, the first image is acquired by only filling even lines of *k*-space, while the second image is acquired by filling the odd lines. Then, both data sets are combined in order to obtain the full *k*-space data that is required for image reconstruction. The key aspect is that each of the sub-sampled data sets is acquired twice as fast as in the single-shot case, which reduces the effective echo spacing by a factor two, and hence also reduces the distortions by a factor of 2. However, one disadvantage of the interleaved EPI approach is that the overall acquisition time is longer than single-shot techniques (because multiple TR intervals are required acquire all data required to form an image). Another disadvantage is that phase errors due to motion (from subject or physiology) can occur between the acquisition of different interleaves, which can lead to severe ghosting artifacts [6].

To overcome the mismatch between different data interleaves, one can acquire navigator echoes that monitor phase errors and correct them before image reconstruction. At their introduction, navigator echoes consisted in single line of *k*-space acquired at the center, which was used to apply a linear phase correction in the readout direction [1, 20]. Later, 2D navigator echoes enabled linear phase correction both in the readout- and in the phase-encoding directions [4]. More recently, non-linear approaches have been introduced [17], which is particularly important for diffusion-weighted imaging of the brain, where cerebrospinal fluid pulsation leads to non-rigid-body brain motion that results in non-linear phase errors if the motion occurs during the application of the diffusion-encoding gradients. 2D non-linear phase correction is most easily applied when each shot in the multi-shot data acquisition samples a contiguous set of data points from a sub-region of *k*-space. In this case, the Nyquist sampling condition is fulfilled and the phase correction can be applied as a complex multiplication in image space. The interleaved EPI sampling scheme does not fulfill this local Nyquist sampling condition and results in aliased signal contributions that complicate the phase correction procedure.

2.1. Readout-segmented EPI

An alternative to the interleaved approach is to perform readout-segmented EPI [25]. In readout-segmented EPI, *k*-space is filled with a series of concatenated segments in the readout direction (Figure 6), corresponding to shorter readout gradient pulses and an overall reduction in the length of the EPI readout As with interleaved EPI, the shorter readout time results in a reduction in the level of susceptibility-based distortion.

2.2. Diffusion-weighted readout-segmented EPI

One advantage of readout-segmented EPI compared to phase-segmented (or interleaved) EPI is that each segment consists of a Nyquist-sampled region of *k*-space that is well suited to the application of 2D non-linear phase correction, as described above. This property of the readout-segmented EPI sampling scheme was first exploited by Porter et al. [24] who proposed the sequence shown in figure 7 for application to diffusion-

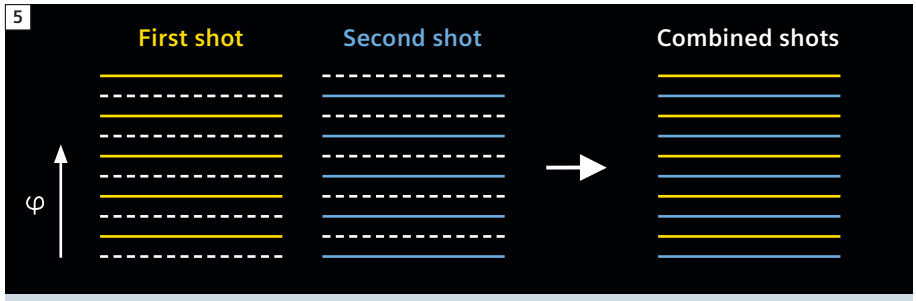

5 Segmented EPI along the phase-encode direction (interleaved EPI). *(I)* Acquire several shots of sub-sampled *k*-space, *(II)* concatenate all shots and *(III)* reconstruct image. Each shot is sub-sampled, resulting in a shorter data sampling interval and reduced distortion.

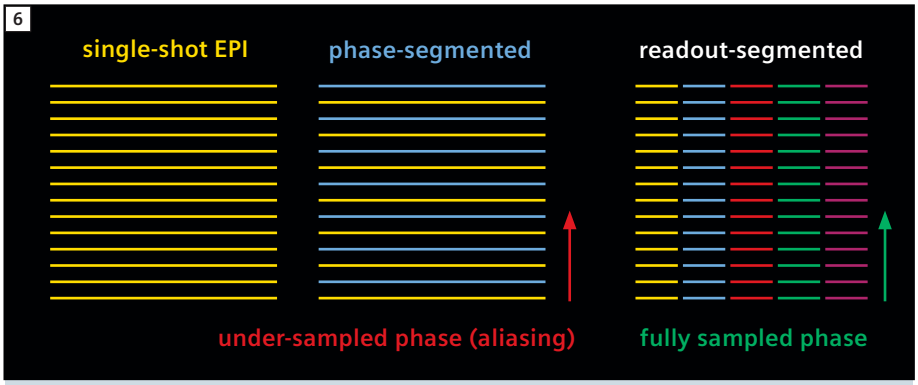

6 Schematic of *k*-space acquired using a conventional single-shot EPI (left), phase-segmented or interleaved EPI (middle) and readout-segmented EPI (right). In the phase-segmented EPI, the data for each shot is sub-sampled in the phase-encoding direction, which induces aliasing and therefore difficulties in correcting for phase-to-phase errors using advanced 2D non-linear techniques. However in readout-segmented EPI, all phase-encode lines are acquired in each shot, therefore there is no aliasing.

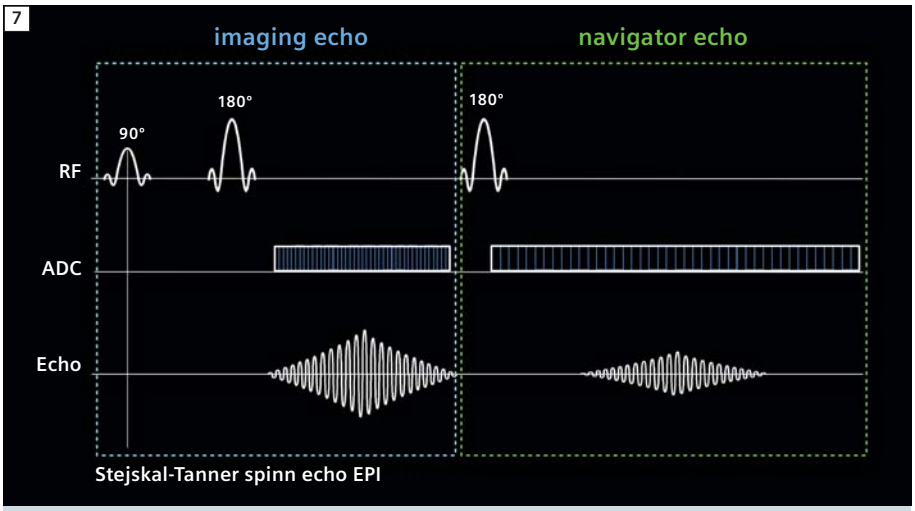

7 Simplified pulse diagram of the RESOLVE sequence (gradients are not represented).

weighted imaging. The sequence consists of an imaging echo, which is used to sample the standard readout-segmented EPI data, and a 2D navigator echo, in which a low resolution EPI readout is used to sample the center of *k*-space at each shot. The sequence was subsequently modified to support parallel imaging [22] using GRAPPA [10]. This made it possible to further shorten the readout time with a corresponding additional reduction in the level of susceptibility artifact. The resulting sequence has been given the acronym RESOLVE[1] (Readout Segmentation Of Long Variable Echo-trains).

2.3. Reacquisition technique

In some cases, the level of motion-induced phase error can be too severe for a reliable phase correction due to signal voids in the navigator images. Although physiological gating strategies can be employed to mitigate these effects, they do not address all sources of motion and can significantly increase acquisition time. To avoid the residual artifacts associated with these occasional extreme phase errors, the RESOLVE[1] sequence uses a reacquisition strategy to identify and re-measure corrupt readout segments that cannot be reliably phase corrected. This method is based on an original concept that was proposed for interleaved EPI and 1D navigator echoes [19], but uses an adapted real-time algorithm, which has been optimized for the combination of 2D navigator data and the readout-segmented EPI sampling scheme [21]. For a comprehensive description of the RESOLVE[1] sequence, including the adaptions for parallel imaging and data reacquisition, the reader is referred to [23].

3. Application of the RESOLVE[1] sequence

To illustrate the benefits of the RESOLVE[1] sequence, Figure 8 shows a comparison between the conventional single-shot EPI (8A) and RESOLVE[1] (8B). Acquisition parameters were:

RESOLVE: Axial slices, TR 3800 ms, TE 80 ms, 4 nex, 12-4 mm thick slices with 0.4 mm gap, 320 × 256 matrix, b=700 s/mm^2 only in slice direction (S-I), GRAPPA x 2, segment 21, FOV 163 mm, acquisition time 6–7 min (depending on reacquisition).

Single-shot EPI: Axial slices, TR 3800 ms, TE 102 ms, 32 nex, 12–4 mm thick slices with 0.4 mm gap, 192 × 192 matrix, b=700 s/mm^2 only in slice direction (S-I), GRAPPA x 2, FOV 220 mm, acquisition time 2 min 15 sec.

All scans were performed at 3T using a 32-channel array head coil.

Images represent an axial mean diffusion-weighted image located in the lower brain region, which is well-known for its susceptibility artifacts due to the sinuses and temporal poles. In the ss-EPI image, strong susceptibility artifacts can be observed as image and signal distortions. For example, the temporal region not only shows image distortion along the phase-encoding direction (antero-posterior), but also shows increase of signal intensity caused by the overlap of distorted voxels (arrow). This spurious signal increase could be falsely interpreted as pathological. Conversely in the RESOLVE[1] image, the same region shows a substantial reduction in this susceptibility artifact. In addition, an overall blurring can be observed on the ss-EPI image, which is caused by the relatively long *k*-space sampling relative to the T2* decay. Reducing the sampling time also reduces this T2* blurring, as can be seen on the RESOLVE[1] image, where the image appears sharper, making it possible to delineated white and gray matter with greater precision.

3.1. 1×1×1 mm^3 resolution full brain at 7T

With the RESOLVE[1] sequence it is possible to acquire high-resolution images without the large increase in susceptibility and T2* artifacts that would affect an ss-EPI acquisition. In one study at 7T, the sequence was used to perform full brain diffusion-weighted imaging at 1×1×1 mm^3 resolution [12]. The study was performed on a whole-body scanner (MAGNETOM 7T[2], Siemens Healthcare, Erlangen, Germany) with a 24-channel RF receive coil (Nova Medical, Wilmington, MA, USA). Acquisition parameters were: 104 axial slices, matrix 220×220, FOV 220 mm, slice thickness 1 mm (no gap), TR 7500 ms, TE 76 ms, 7 readout segments, 30 diffusion-weighting directions at a b-value of 1000 s/mm^2, acquisition time was 78 min. The diffusion-weighted images were filtered with a two-stage hybrid image restoration procedure, corrected for subject motion and registered to a T1-weighted anatomical image (1 mm resolution) of the same participant. For each voxel, multiple fiber orientations were modeled by constrained spherical deconvolution [30] followed by whole-brain fiber-tracking using

MRtrix (http://www.brain.org.au/software)[3].
Figure 9 shows results of the fiber orientation distribution function (ODF) and tractography centered over the pre-motor cortex. The spatial consistency of the fiber ODF demonstrates the high SNR of the data (Figure 9B). Tractography successfully demonstrated intersection of the corpus callosum (CC, pink), the corona radiata (CR, blue) and the superior longitudinal fasciculus (SLF, green, tracks not shown).
The same data were processed using track-density imaging [5], which makes it possible to reconstruct fiber bundles at 200 µm resolution. Figure 10 shows the results at the three orientations in order to appreciate the 1 mm isotropic resolution. The views are centered over the thalamus. The ultra-high resolution in combination with high SNR and low susceptibility artifacts provide an unprecedented level of detail about the anatomical organization of the thalamus. The ability of the sequence to provide full brain coverage at an isotropic resolution of 1 mm made it possible to reconstruct track density images of the whole brain with no orientation bias.

3.2. Spinal cord DTI at 3T

Another powerful application of the RESOLVE sequence is the spinal cord. Indeed, spinal cord DTI is particularly challenging due to *(I)* the small cross-sectional size of the spinal cord, which requires high spatial resolution, resulting in low SNR at standard imaging times; *(II)* susceptibility artifacts, which are caused by inhomogeneous magnetic field in the spinal region due to the close proximity of tissue with very different magnetic susceptibility (tissue, bone, air, cartilage) and *(III)* physiological-related motion due to respiration, heart beat, cerebrospinal fluid pulsation. The first two arguments (small size and susceptibility artifacts) are particularly well suited for the RESOLVE[1] sequence, as this

[3]MRtrix is not a Siemens Healthcare product. Siemens bears no responsibility for this product including, but not limited to, its regulatory status. Further information about the software can be found at the website listed.

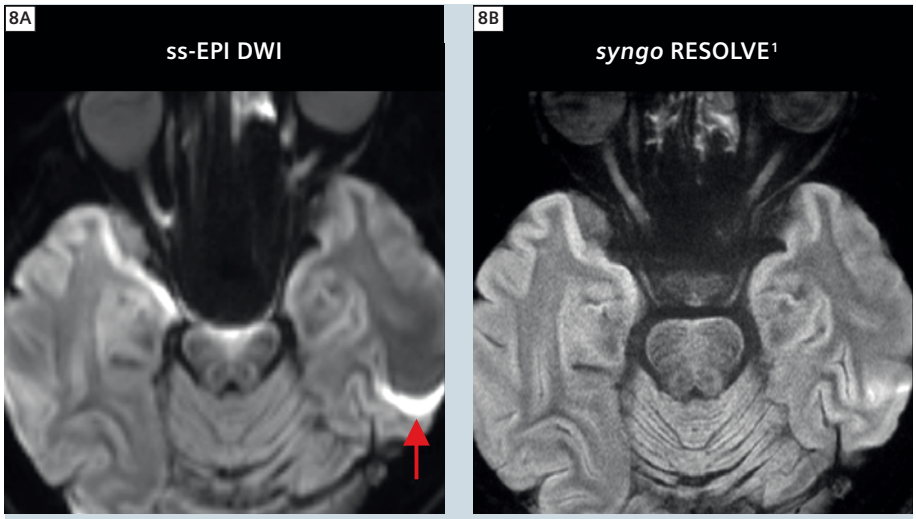

8 Comparison of standard single-shot EPI sequence **(8A)** and *syngo* RESOLVE[1] **(8B)**. Susceptibility distortions are substantially reduced on the RESOLVE[1] image. For example, the temporal region of the ss-EPI image not only shows image distortion along the phase-encoding direction (antero-posterior), but also shows an increase in signal intensity caused by the overlap of distorted voxels (arrow). Sharper image with RESOLVE[1] also comes from faster sampling, via reduction of T2* blurring. *Images courtesy of Professor Naganawa, Nagoya University School of Medicine, Japan.*

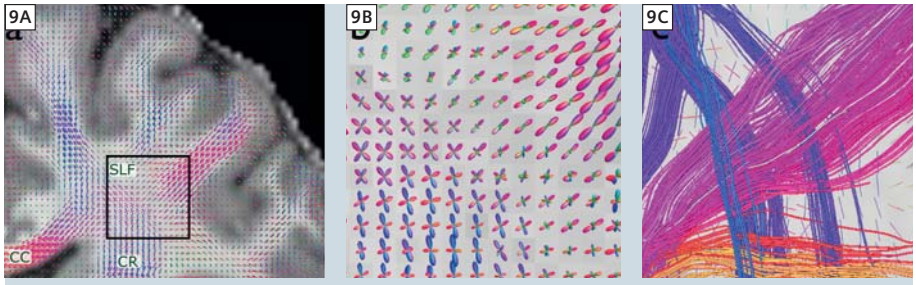

9 High angular resolution diffusion imaging results from 1 mm isotropic resolution. **(9A)** Coronal view centered in the pre-motor region at the intersection between corpus callosum (CC), superior longitudinal fasciculus (SLF) and corona radiate (CR). **(9B)** Orientation distribution functions (ODF) showing crossing of the major pathways. **(9C)** Tractography results showing intersection of the CC (pink) and CR (blue). *Images courtesy of Drs. Robin Heidemann and Alfred Anwander, MPI Leipzig, Germany.*

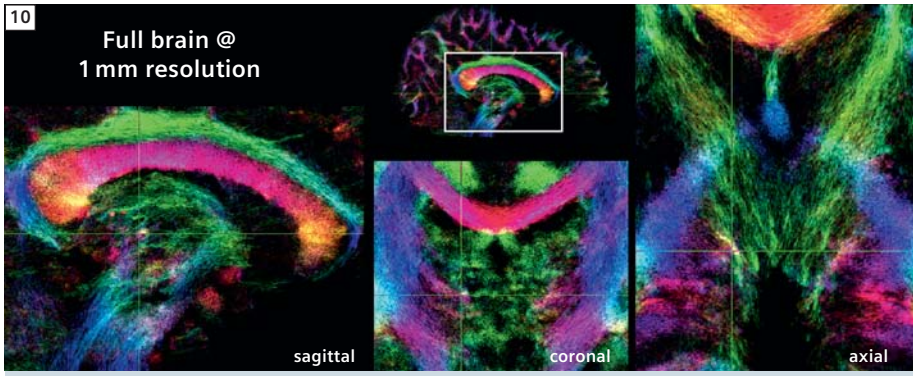

10 Track density image with 200 µm resolution. Fine details of the structure of the thalamus are visible. *Image courtesy of Drs. Robin Heidemann and Alfred Anwander, MPI Leipzig, Germany.*

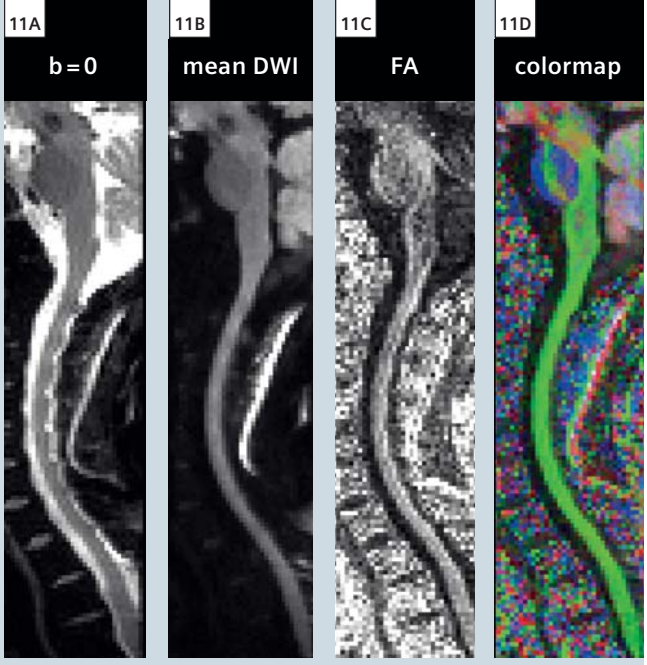

11 Human cervical spinal cord. 1.7 mm isotropic, 3 shots, R = 3, TE 74 ms, Cardiac gating, b 800 s/mm², 30 directions in 8 min.

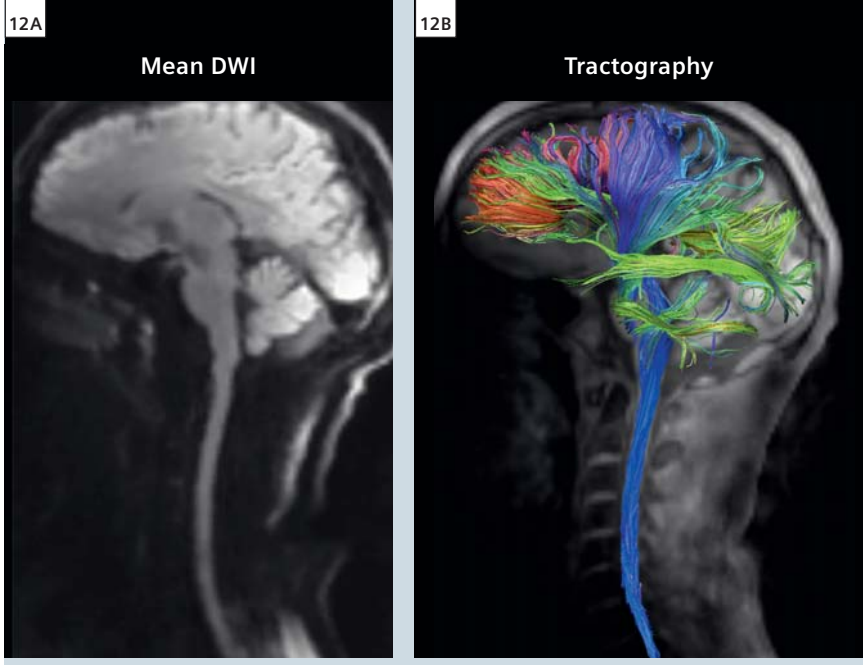

12 Sagittal view of the mean diffusion-weighted images **(12A)** and fiber tractography overlaid on the anatomical image **(12B)**. Almost no distortions are observed, which makes it possible to explore white matter connections from cortical areas down to the spinal cord without spurious interruptions.

sequence provides high SNR and enables reduction of susceptibility distortions. The last challenge (physiological motion) is a typical cause of failure for segmented approaches, however the non-linear 2D phase correction combined with the reacquisition scheme enabled in the RESOLVE[1] sequence ensures low sensitivity to physiological motion.

An example of the RESOLVE[1] in the spinal cord is shown in Figure 11. To further improve image quality, the RESOLVE[1] sequence was used with parallel imaging using the GRAPPA algorithm [10] to further reduce susceptibility artifacts and shorten the TE. To maximize the capabilities of parallel imaging, a dedicated 32-channel head/spine coil was used, which enables up to 4× acceleration [9]. Acquisition parameters were: 1.7 mm isotropic, 3 shots, R = 3 acceleration (iPAT3), TE 74 ms, Cardiac gating, b 800 s/mm², 30 directions, acquisition time 8 min. The sequence only used 3 shots (i.e., 3 segments per *k*-space), therefore the acquisition was relatively short. Although minor distortions are still visible on the b = 0 image at the level of each intervertebral disk, the spinal cord itself is not affected by these intervertebral distortions as assessed by the mean diffusion-weighted image, the fractional anisotropy (FA) map and the FA color map. Note the particularly high spatial resolution (1.7 mm isotropic, 4.9 mm³ voxel volume), which is rarely achieved in spinal cord imaging.

One particularly difficult acquisition is when one wants to image the full brain and spinal cord. The challenge of B_0-inhomogeneity can be partially overcome when only the spinal cord is imaged by adjusting the shim volume within an elongated box that nicely encompasses the spinal cord. However, when the FOV includes both the brain and spinal cord, it is a difficult for the shimming algorithm to find appropriate fitting coefficients for ensuring B_0-homogeneity both in the brain and spinal cord, due to the complex geometry and the presence of several susceptibility interfaces (sinuses, temporal poles, brainstem, intervertebral disks and lungs). This type of acquisition is therefore particularly well-suited to the RESOLVE[1] sequence.

Images were acquired with the following parameters: 2.2 mm isotropic resolution, matrix 138 × 104, TR ~ 15000 ms (cardiac gating), TE 66 ms, 3 shots, R = 3 acceleration, b 800 s/mm², 30 diffusion-weighting directions, acquisition time 10:45 min. Images were further corrected for residual susceptibility-distortions in the thoracic region (due to the close proximity with the lungs), using the reversed gradient technique [13]. Tractography was performed using the Diffusion Toolkit[3] (deterministic FACT algorithm) and displayed with TrackVis[3] (http://www.trackvis.org/). Diffusion-weighted images were then registered to the 1 mm isotropic anatomical image (MPRAGE). Results are shown in Figure 12 and demonstrate reduction of susceptibility artifacts, enabling to explore connections within and between the brain, brainstem and cervical spinal cord.

4. Conclusion

syngo RESOLVE[1] is a useful sequence for acquiring high-quality diffusion-weighted images thanks to the reduction of susceptibility distortion, reduction of T2* blurring, shorter TE (and hence high SNR) and robust correction for motion-induced artifacts. The RESOLVE sequence has shown promising tractography results in the brain and spinal cord, the latter being known for suffering from severe susceptibility artifacts using standard sequences. The RESOLVE sequence can be combined with other acquisition strategies such as reduced field-of-view and parallel imaging. Potential applica-

[3]Diffusion Toolkit and TrackVis are not Siemens Healthcare products. Siemens bears no responsibility for these products including, but not limited to, their regulatory status. Further information about the software can be found at the website listed.

tions in research include the study of white matter architecture in the brain, brainstem and spinal cord, and also the possibility to study fine structure such as the thalamus and the gray nuclei. In clinical application, the reduced level of susceptibility artifact with the RESOLVE[1] sequence can provide better interpretation of abnormalities in white matter pathology. Although acceptable image quality can already be obtained using the conventional single-shot EPI sequence providing shimming is successful, this procedure is strongly user-dependent, subject-dependent and structure-dependent. Because this variability is not acceptable in clinical routine, the RESOLVE[1] sequence has the potential to ensure robust image quality. Moreover, the RESOLVE[1] sequence may be particularly useful in cases where patients have metallic implants, notably in spinal cord injury, where assessing the integrity of spinal pathway would be of tremendous help for patient prognosis.

5. Acknowledgements

The author wishes to thank Drs. Lawrence Wald, Thomas Witzel, Kawin Setsompop and Boris Keil at the *A. A. Martinos Center for Biomedical Imaging*, Alfred Anwander at the *Max Planck Institut* and Drs. David Porter, Keith Heberlein, Himanshu Bhat, Robin Heidemann and Ignacio Vallines at *Siemens Healthcare*. This study was supported by NIH-P41RR14075 and National Multiple Sclerosis Society (FG 1892A1/1).

[1]The software is pending 510(k) clearance, and is not yet commercially available in the United States and in other countries.

[2]The 7T system is a research system only. It cannot be used outside of a research study.

References

1 Anderson, A.W., Gore, J.C., 1994. Analysis and correction of motion artifacts in diffusion weighted imaging. Magn Reson Med 32, 379-387.

2 Basser, P.J., Mattiello, J., LeBihan, D., 1994. Estimation of the effective self-diffusion tensor from the NMR spin echo. J Magn Reson 103, 247-254.

3 Beaulieu, C., 2002. The basis of anisotropic water diffusion in the nervous system – a technical review. NMR Biomed 15, 435-455.

4 Butts, K., Pauly, J., de Crespigny, A., Moseley, M., 1997. Isotropic diffusion-weighted and spiral-navigated interleaved EPI for routine imaging of acute stroke. Magn Reson Med 38, 741-749.

5 Calamante, F., Tournier, J.-D., Jackson, G.D., Connelly, A., 2010. Track-density imaging (TDI): super-resolution white matter imaging using whole-brain track-density mapping. NeuroImage 53, 1233-1243.

6 Clark, C.A., Barker, G.J., Tofts, P.S., 2000. Improved reduction of motion artifacts in diffusion imaging using navigator echoes and velocity compensation. J Magn Reson 142, 358-363.

7 Cohen-Adad, J., El Mendili, M.-M., Lehéricy, S., Pradat, P.-F., Blancho, S., Rossignol, S., Benali, H., 2011a. Demyelination and degeneration in the injured human spinal cord detected with diffusion and magnetization transfer MRI. NeuroImage 55, 1024-1033.

8 Cohen-Adad, J., El Mendili, M.M., Morizot-Koutlidis, R., Lehericy, S., Meininger, V., Blancho, S., Rossignol, S., Benali, H., Pradat, P.-F., 2012. Involvement of spinal sensory pathway in ALS and specificity of cord atrophy to lower motor neuron degeneration. Amyotroph Lateral Scler doi:10.3109/17482968.2012.701308.

9 Cohen-Adad, J., Mareyam, A., Keil, B., Polimeni, J.R., Wald, L.L., 2011b. 32-channel RF coil optimized for brain and cervical spinal cord at 3 T. Magn Reson Med 66, 1198-1208.

10 Griswold, M.A., Jakob, P.M., Heidemann, R.M., Nittka, M., Jellus, V., Wang, J., Kiefer, B., Haase, A., 2002. Generalized autocalibrating partially parallel acquisitions (GRAPPA). Magn Reson Med 47, 1202-1210.

11 Hagmann, P., Jonasson, L., Maeder, P., Thiran, J.P., Wedeen, V.J., Meuli, R., 2006. Understanding diffusion MR imaging techniques: from scalar diffusion-weighted imaging to diffusion tensor imaging and beyond. Radiographics 26 Suppl 1, S205-223.

12 Heidemann, R.M., Porter, D.A., Anwander, A., Feiweier, T., Calamante, F., Tournier, J.-D., Lohmann, G., Meyer, H., Knoesche, T.R., Turner, R., 2011. Whole-Brain, Multi-Shot, Diffusion-Weighted Imaging in Humans at 7T with 1 mm Isotropic Resolution. Proceedings of the 19th Annual Meeting of ISMRM, Montreal, Canada 541.

13 Holland, D., Kuperman, J.M., Dale, A.M., 2010. Efficient correction of inhomogeneous static magnetic field-induced distortion in Echo Planar Imaging. NeuroImage 50, 175-183.

14 Johansen-Berg, H., Behrens, T.E., 2006. Just pretty pictures? What diffusion tractography can add in clinical neuroscience. Curr Opin Neurol 19, 379-385.

15 Le Bihan, D., Mangin, J.F., Poupon, C., Clark, C.A., Pappata, S., Molko, N., Chabriat, H., 2001. Diffusion tensor imaging: concepts and applications. J Magn Reson Imaging 13, 534-546.

16 Mansfield, P., 1977. Multi-planar image formation using NMR spin echoes. J. Phys. C: Solid State Phys. 10, L55-58.

17 Miller, K.L., Pauly, J.M., 2003. Nonlinear phase correction for navigated diffusion imaging. Magn Reson Med 50, 343-353.

18 Mori, S., Zhang, J., 2006. Principles of diffusion tensor imaging and its applications to basic neuroscience research. Neuron 51, 527-539.

19 Nguyen, Q., Clemence, M., Thornton, J., Ordidge, R., 1999. Isotropic diffusion-weighted multishot imaging using automatic reacquisition. Proceedings of the 7th Annual Meeting of ISMRM, Philadelphia, USA, 559.

20 Ordidge, R.J., Helpern, J.A., Qing, Z.X., Knight, R.A., Nagesh, V., 1994. Correction of motional artifacts in diffusion-weighted MR images using navigator echoes. Magn Reson Imaging 12, 455-460.

21 Porter, D.A., 2006. 2D-navigator-based re-acquisition for motion artefact suppression in multi-Shot, diffusion-weighted Imaging. Proceedings of the 14th Annual Meeting of ISMRM, Seattle, USA, 1047.

22 Porter, D.A., Heidemann, R., 2006. Multi-Shot, Diffusion-Weighted Imaging at 3T using readout-segmented EPI and GRAPPA. Proceedings of the 14th Annual Meeting of ISMRM, Seattle, USA, 1046.

23 Porter, D.A., Heidemann, R.M., 2009. High resolution diffusion-weighted imaging using readout-segmented echo-planar imaging, parallel imaging and a two-dimensional navigator-based reacquisition. Magn Reson Med 62, 468-475.

24 Porter, D.A., Mueller, E., 2004. Multi-shot diffusion-weighted EPI with readout mosaic segmentation and 2D navigator correction. Proceedings of the 12th Annual Meeting of ISMRM, Kyoto, Japan, 442.

25 Robson, M.D., Anderson, A.W., Gore, J.C., 1997. Diffusion-weighted multiple shot echo planar imaging of humans without navigation. Magn Reson Med 38, 82-88.

26 Schmierer, K., Wheeler-Kingshott, C.A.M., Boulby, P.A., Scaravilli, F., Altmann, D.R., Barker, G.J., Tofts, P.S., Miller, D.H., 2007. Diffusion tensor imaging of post mortem multiple sclerosis brain. NeuroImage 35, 467-477.

27 Schwartz, E.D., Duda, J., Shumsky, J.S., Cooper, E.T., Gee, J., 2005. Spinal cord diffusion tensor imaging and fiber tracking can identify white matter tract disruption and glial scar orientation following lateral funiculotomy. J Neurotrauma 22, 1388-1398.

28 Song, S.K., Sun, S.W., Ju, W.K., Lin, S.J., Cross, A.H., Neufeld, A.H., 2003. Diffusion tensor imaging detects and differentiates axon and myelin degeneration in mouse optic nerve after retinal ischemia. NeuroImage 20, 1714-1722.

29 Stejskal, E.O., Tanner, J.E., 1965. Spin Diffusion Measurements: Spin Echoes in the Presence of a Time-Dependent Field Gradient. J Chem Phys 42, 288-292.

30 Tournier, J.D., Calamante, F., Connelly, A., 2007. Robust determination of the fibre orientation distribution in diffusion MRI: non-negativity constrained super-resolved spherical deconvolution. NeuroImage 35, 1459-1472.

31 Turner, R., Le Bihan, D., 1990. Single-shot diffusion imaging at 2.0 Tesla. J Magn Reson 86, 445-452.

Contact
Julien Cohen-Adad, Ph.D.
Department of Electrical Engineering
Ecole Polytechnique de Montreal
2900 Edouard-Montpetit Bld.
Montreal, QC, H3T 1J4
Canada
Phone: +1 514-340-4711
Fax: +1 514-340-4611
jcohen@polymtl.ca